Self-Assembly Behavior of Amphiphilic Block Copolymer/Nanoparticle Mixture in Dilute Solution Studied by Self-Consistent-Field Theory/Density Functional Theory

Liangshun Zhang, Jiaping Lin,* and Shaoliang Lin

Key Laboratory for Ultrafine Materials of Ministry of Education, School of Materials Science and Engineering, East China University of Science and Technology, Shanghai 200237, China

Received April 30, 2007; Revised Manuscript Received May 28, 2007

ABSTRACT: A theoretical approach combining self-consistent-field theory (SCFT) for fluids and density functional theory (DFT) for particles was applied to investigate the self-assembly behavior of amphiphilic diblock copolymer/nanoparticle mixture in dilute solution. Two kinds of hydrophobic nanoparticles are studied: one is that the particles are selective to hydrophobic blocks but are incompatible with hydrophilic blocks, and the other is that the particles are nonselective to hydrophobic and hydrophilic blocks. For both cases, the self-association of amphiphilic block copolymer/nanoparticle mixture is observed, and the nanoparticles are spatially organized in the clusters. The aggregate morphologies can be tuned by the particle radius and particle volume fraction. For the selective particles, the aggregate morphologies of amphiphilic block copolymer/nanoparticle mixture can experience a transition from vesicles to mixture of circlelike and rod micelles as the particle radius and/or particle volume fraction increase. For the nonselective nanoparticles, the large compound micelles are produced instead of the vesicles. The large compound micelles transform to the mixture of large compound micelles and circlelike micelles with an increase in particle volume fraction and/or radius. The distribution of nanoparticles in the clusters is also affected by the particle radius and volume fraction. For both cases, when the values of nanoparticle radius and/or volume fraction are small, the nanoparticles are almost uniformly distributed in the cores of micelles. However, the particles tend to localize near the interfaces between the core and shell with increasing particle volume fraction and/or radius.

Introduction

Amphiphilic block copolymers can self-assemble into micelles with controllable sizes and morphologies in selective solvent,[1,2] such as rodlike micelles, spherelike micelles, and vesicles. This allows them to serve as templates for controlling the nanoparticle organization. Throughout the self-assembly of the amphiphilic block copolymer/nanoparticle mixture in selective solvent, the nanoparticles can be spatially organized in the formed aggregates. These microstructure materials have attracted considerable attention due to their unique electronic, magnetic, and optical properties and potential applications, such as catalysis, semiconductor, and photonic and biomimetic materials, which strongly depend on the size and organization of the nanoparticles.[3−6]

Recently, the self-assembly behavior of amphiphilic block copolymer/nanoparticle mixture was experimentally reported by many research groups.[7−18] The mixture can self-associate into the complex microstructures in selective solvent. The hydrophilic blocks form the corona, which provides the stabilization, while the hydrophobic blocks produce the core isolating the nanoparticles from the solvent. For example, Taton et al. reported that the amphiphilic block copolymers poly(styrene-*b*-acrylic acid) can assemble around gold, magnetic, and semiconductor nanoparticles to encapsulate the particles within the micelles.[7−10] The hydrophobic styrene cores physically sequester the nanoparticles from the aqueous solution. Meanwhile, the nanoparticles can also have an impact on the supramolecular structures of block copolymers, and the incorporation of nanoparticles has been found to lead to the morphology transition of parent block copolymers.[19−21] The chemical and physical properties of copolymer−nanoparticle structures can be tuned by the morphologies of block copolymer aggregates and the distributions of particles, which depend on the concentrations of copolymers and particles, the size and shape of particles, the selectivity of particles, etc.

The real space implemented self-consistent-field theory (SCFT) was successfully used to explore the cornucopian morphologies assembled by complex architecture copolymers in bulk.[22−26] For the study of the complex microstructures, a prior assumption about the morphology is not necessary. This method is found to be an efficient way to tackle the problem of self-assembled complex structures in dilute copolymer solution.[27−31] Recently, Liang et al. first extended this method to investigate the aggregation behavior of amphiphilic diblock copolymers in dilute solution.[27,28] Complex micelles (e.g., spherelike micelles and rodlike micelles) and vesicles were obtained by tailoring the interaction parameters, initial density fluctuation, and polydispersity. This method was also used to investigate the self-assembly morphologies of amphiphilic ABC linear triblock copolymers and star triblock copolymers in solution by Yang's group.[29,30] Various micelle structures, such as hamburger, segmented wormlike, and toroidal segmented micelles, have been observed. We utilized SCFT to investigate the effect of architecture parameters of graft copolymers on their self-assembly behavior.[31] The morphology transitions among circlelike micelles, linelike micelles, and vesicles can be triggered by changing the branch number and graft position of graft copolymers. These simulation results are in good agreement with the experimental observations.

Various tools have been used to study the mixture of block copolymers and nanoparticles in bulk, such as self-consistent-field theory/density functional theory,[32−37] self-consistent-field theory,[38,39] hybrid field theory,[40] Monte Carlo,[41,42] dissipative

* Corresponding author: Tel +86-21-64253370; Fax +86-21-64253539; e-mail jplinlab@online.sh.cn.

10.1021/ma070986y CCC: $37.00
Published on Web 06/29/2007

particle dynamics,[43] molecular dynamics,[44] and strong segregation theory.[41,43−46] Among these methods, field theory is a powerful technique for characterizing the system. Balazs and co-workers developed a theoretical approach for calculating the morphology and thermodynamic behavior of block copolymer/nanoparticle mixture without requiring a priori knowledge of the equilibrium structures.[32−35] This approach combines a self-consistent-field theory (SCFT) for polymers and a density functional theory (DFT) for particles. SCFT was used to characterize the equilibrium thermodynamical features of polymer systems, while DFT captures the particle ordering and phase behavior in colloidal systems. They found that the morphologies of diblock copolymers and distributions of particles can be tailored by the concentration of adding particles, the size of particles, the interaction between the particles and blocks, and the polydispersity of particles. They also have the conclusion that the incorporation of nanoparticles can lead to the morphology transition of block copolymers between cylindrical and lamellar phases. Although these theoretical studies have successfully predicted the self-assembly behavior of the block copolymer/nanoparticle mixture, the understanding of physical mechanism that drives the self-assembly of amphiphilic block copolymer/nanoparticle mixture in dilute solution is still lacking.

The purpose of the present work is to investigate the aggregation behavior of amphiphilic block copolymer/nanoparticle mixture in dilute solution and the spatial organization of nanoparticles in the clusters. The SCFT/DFT framework developed by Balazs et al. is extended to study the amphiphilic block copolymer/nanoparticle mixture in dilute solution. As far as we know, the self-assembly behavior of the system in dilute solution has not yet been studied by the SCFT/DFT methodology. It is demonstrated that the amphiphilic block copolymer/nanoparticle mixture can form aggregates with various shapes in dilute solution. The nanoparticles are encapsulated inside the clusters. The particle volume fraction and particle radius have a remarkable effect on the morphologies of aggregates and particle distributions. On the basis of these results, phase diagrams were constructed, which display the stability regions of microstructures as functions of the particle radius and particle volume fraction. We expect that the present study may offer a mechanism toward efficiently understanding the self-assembly behavior of amphiphilic block copolymer/nanoparticle mixture in dilute solution.

Theoretical Model

A recent numerical approach developed by Balazs and co-workers has addressed the polymer nanoparticle composites by coupling SCFT for inhomogeneous polymeric fluids with DFT for hard spheres to account for steric packing effects of particles.[32−35] The integrated SCFT/DFT technique identifies new self-assembly morphologies of the blend of diblock copolymers and nanoparticles, where the particles and copolymers can organize into mesoscopically regular patterns. A powerful feature of this method is that priori assumptions about the morphology and the distribution of particles are not necessary. In our model, we extend the SCFT/DFT scheme to describe the mixture of amphiphilic block copolymers and particles in solution. The contribution from the solvent molecules is included in the theory framework. Below, we provide a brief description of the model we used to probe the self-assembly behavior of amphiphilic block copolymer/nanoparticle mixture in solution.

We consider a system with volume V, containing n_D AB diblock copolymers, n_S solvent molecules (S), and n_P hard spherical particles (P). All the diblock copolymer chains in solution are flexible. Each copolymer is composed of N total segments. The segment volumes and statistical lengths for both monomer A and B are denoted by ρ_0^{-1} and a, respectively. f_A denotes the volume fraction of A-type segment per chain. The solvent molecule has the same volume with the segment of copolymer. All particles have the same radius R_P. The volume fractions of particles and diblock copolymers in solution are c_P and c_D, respectively, and that of solvent is $c_S = 1 - c_P - c_D$.

Within mean-field theory, the pair interactions between different components are determined by a set of effect chemical potential fields $\omega_K(\mathbf{r})$ (K = A, B, P, S), replacing actual interactions within solution. The free energy of the amphiphilic block copolymer/nanoparticle/solvent system is given by

$$\frac{NF}{\rho_0 k_B T V} = -\frac{c_P}{\alpha}\ln\left(\frac{Q_P \alpha}{V c_P}\right) - c_D \ln\left(\frac{Q_D}{V c_D}\right) - c_S N \ln\left(\frac{Q_S}{V c_S}\right) + \frac{1}{V}\int d\mathbf{r}\left[\frac{1}{2}\sum_{\substack{u,v=A,B,P,S \\ u\neq v}} \chi_{uv} N \phi_u(\mathbf{r})\,\phi_v(\mathbf{r}) - \sum_{u=A,B,S} \omega_u(\mathbf{r})\,\phi_u(\mathbf{r}) - \omega_P(\mathbf{r})\,\rho_P(\mathbf{r}) - \xi(\mathbf{r})\left(1 - \sum_{u=A,B,P,S}\phi_u(\mathbf{r})\right)\right] + \frac{1}{V}\int d\mathbf{r}\,\rho_P(\mathbf{r})\,\Psi_{HS}(\bar{\phi}_P(\mathbf{r})) \quad (1)$$

where k_B is Boltzmann's constant and T is the temperature. α is the volume ratio of the particle with radius R_P to block copolymer chain, defined by

$$\alpha \equiv \frac{v_R \rho_0}{N} = \frac{4\pi}{3}\left(\frac{R_P}{R_g}\right)^3 (\bar{N})^{1/2} \quad (2)$$

where $R_g = N\sqrt{a/6}$ is the ideal gyration radius of the diblock copolymer, $\bar{N} \equiv a^6\rho^2 N/6^3$ is the invariant polymerization index, and $v_R = 4\pi R_P^3/3$ is the volume of particle with radius R_P. Here, $\phi_A(\mathbf{r})$, $\phi_B(\mathbf{r})$, $\phi_S(\mathbf{r})$, and $\phi_P(\mathbf{r})$, which correspond to the density fields, are the local volume fractions of A segments, B segments, solvent, and particles, respectively. $\xi(\mathbf{r})$ is the potential field that is invoked by incompressibility condition ($\phi_A(\mathbf{r}) + \phi_B(\mathbf{r}) + \phi_P(\mathbf{r}) + \phi_S(\mathbf{r}) = 1$). χ_{IJ} characterize the interactions between species I and J. $\rho_P(\mathbf{r})$ is the particle center distribution. The local particle volume fraction $\phi_P(\mathbf{r})$ is given by

$$\phi_P(\mathbf{r}) = \frac{\alpha}{v_R}\int_{|\mathbf{r}'|<R} d\mathbf{r}'\,\rho_P(\mathbf{r}+\mathbf{r}') \quad (3)$$

Q_S is the partition function of a solvent in the field $\omega_S(\mathbf{r})$ given by

$$Q_S = \int d\mathbf{r}\,\exp\left(-\frac{\omega_S(\mathbf{r})}{N}\right) \quad (4)$$

Q_P is the partition function of a single particle subject to the field $\omega_P(\mathbf{r})$

$$Q_P = \int d\mathbf{r}\,\exp(-\omega_P(\mathbf{r})) \quad (5)$$

$Q_D = \int d\mathbf{r}\, q(\mathbf{r},s)\, q^+(\mathbf{r},1-s)$ is the partition function for a single noninteracting diblock copolymer chain subject to fields $\omega_A(\mathbf{r})$ and $\omega_B(\mathbf{r})$. The contour length s increases continuously from 0 to 1 as the block changes from one end to the other. The spatial coordinate $\mathbf{r}$ is in units of R_g. The propagator $q(\mathbf{r},s)$ represents

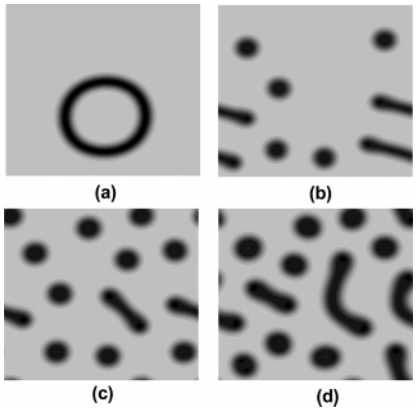

Figure 1. Two-dimensional density distributions of particles in the amphiphilic block copolymer/particle solutions with particle radius $R_P/R_g = 0.70$ and particle volume fractions $c_P = 0.020$ (a), $c_P = 0.030$ (b), $c_P = 0.050$ (c), and $c_P = 0.080$ (d). Light gray regions represent low local volume fraction of particles, while black regions indicate high local volume fraction of particles.

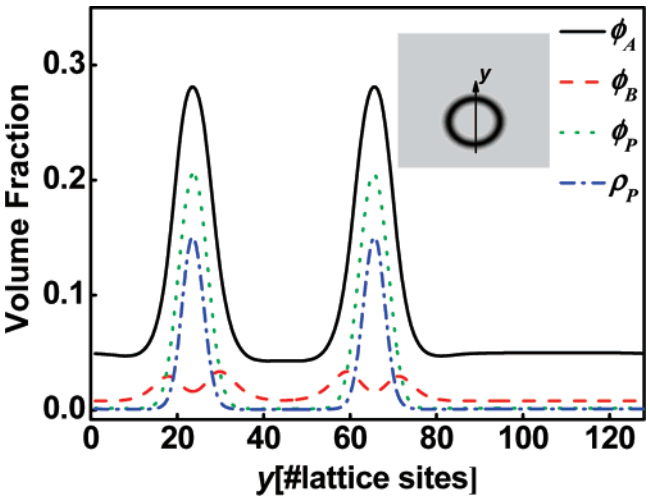

Figure 2. Distribution profiles of hydrophobic blocks ϕ_A, hydrophilic blocks ϕ_B, particles ϕ_P, and particle centers ρ_P on a cross section of the vesicle marked with an arrow in the inset for $R_P/R_g = 0.70$ and $c_P = 0.020$. The inset is a two-dimensional density distribution of particles.

the probability of finding segments s at position $\mathbf{r}$, which satisfies the modified diffusion equation

$$\frac{\partial q(\mathbf{r},s)}{\partial s} = \nabla^2 q(\mathbf{r},s) - \omega(\mathbf{r})\, q(\mathbf{r},s) \tag{6}$$

subject to the initial condition $q(\mathbf{r},0) = 1$ and with $\omega(\mathbf{r}) = \omega_A(\mathbf{r})$ when $0 < s < f$ and $\omega(\mathbf{r}) = \omega_B(\mathbf{r})$ when $f < s < 1$. The backward propagator $q^+(\mathbf{r},s)$ satisfies eq 6 subject to the initial condition $q^+(\mathbf{r},0) = 1$ and with $\omega(\mathbf{r}) = \omega_B(\mathbf{r})$ when $0 < s < 1 - f$ and $\omega(\mathbf{r}) = \omega_A(\mathbf{r})$ when $1 - f < s < 1$. The last term of eq 1 describes the steric free energy of the particles according to Carnahan−Starling function[47,48]

$$\Psi_{HS}(x) = \frac{4x - 3x^2}{(1-x)^2} \tag{7}$$

with the weighted nonlocal volume fraction $\bar{\phi}_P(\mathbf{r})$ of particles

$$\bar{\phi}_P(\mathbf{r}) = \frac{\alpha}{v_{2R}} \int_{|\mathbf{r}'|<2R} d\mathbf{r}'\, \rho_P(\mathbf{r}+\mathbf{r}') \tag{8}$$

where v_{2R} is the volume of a sphere with radius $2R_P$.

The minimization of free energy F, with respect to $\phi_A(\mathbf{r})$, $\phi_B(\mathbf{r})$, $\phi_S(\mathbf{r})$, $\rho_P(\mathbf{r})$, $\omega_A(\mathbf{r})$, $\omega_B(\mathbf{r})$, $\omega_S(\mathbf{r})$, $\omega_P(\mathbf{r})$, and $\xi(\mathbf{r})$, can lead to a set of mean-field equations:

$$\omega_A(\mathbf{r}) = \chi_{AB}N\phi_B(\mathbf{r}) + \chi_{AP}N\phi_P(\mathbf{r}) + \chi_{AS}N\phi_S(\mathbf{r}) + \xi(\mathbf{r}) \tag{9}$$

$$\omega_B(\mathbf{r}) = \chi_{AB}N\phi_A(\mathbf{r}) + \chi_{BP}N\phi_P(\mathbf{r}) + \chi_{BS}N\phi_S(\mathbf{r}) + \xi(\mathbf{r}) \tag{10}$$

$$\omega_S(\mathbf{r}) = \chi_{AS}N\phi_A(\mathbf{r}) + \chi_{BS}N\phi_B(\mathbf{r}) + \chi_{PS}N\phi_P(\mathbf{r}) + \xi(\mathbf{r}) \tag{11}$$

$$\omega_P(\mathbf{r}) = \Psi_{HS}(\bar{\phi}_P(\mathbf{r})) + \frac{\alpha}{v_{2R}} \int_{|\mathbf{r}'|<2R} d\mathbf{r}'\, \rho_P(\mathbf{r}+\mathbf{r}')\Psi'_{HS}(\bar{\phi}_P(\mathbf{r}+\mathbf{r}')) + \frac{\alpha}{v_R} \int_{|\mathbf{r}'|<R} d\mathbf{r}' \,[\chi_{AP}N\phi_A(\mathbf{r}+\mathbf{r}') + \chi_{BP}N\phi_B(\mathbf{r}+\mathbf{r}') + \chi_{PS}N\phi_S(\mathbf{r}+\mathbf{r}') + \xi(\mathbf{r}+\mathbf{r}')] \tag{12}$$

where

$$\Psi'_{HS}(x) = \frac{d\Psi_{HS}(x)}{dx}$$

$$\phi_A(\mathbf{r}) = \frac{Vc_D}{Q_D} \int_0^f ds\, q(\mathbf{r},s)\, q^+(\mathbf{r},1-s) \tag{13}$$

$$\phi_B(\mathbf{r}) = \frac{Vc_D}{Q_D} \int_f^1 ds\, q(\mathbf{r},s)\, q^+(\mathbf{r},1-s) \tag{14}$$

$$\phi_S(\mathbf{r}) = \frac{Vc_S}{Q_S} \exp\left(-\frac{\omega_S(\mathbf{r})}{N}\right) \tag{15}$$

$$\rho_P(\mathbf{r}) = \frac{Vc_P}{Q_P\alpha} \exp(-\omega_P(\mathbf{r})) \tag{16}$$

$$\phi_A(\mathbf{r}) + \phi_B(\mathbf{r}) + \phi_P(\mathbf{r}) + \phi_S(\mathbf{r}) = 1 \tag{17}$$

To solve the SCFT equations, we use a variant of algorithm developed by Fredrickson and co-workers.[22−25] The initial values of the density fields $\phi_I(\mathbf{r})$ (I = A, B, S) satisfy the Gaussian distributions:[27]

$$\langle \phi_I(\mathbf{r}) - c_I \rangle = 0$$

$$\langle (\phi_I(\mathbf{r}) - c_I)(\phi_J(\mathbf{r}') - c_J) \rangle = \beta c_I c_J \delta_{IJ} \delta(\mathbf{r} - \mathbf{r}') \tag{18}$$

Here, β characterizes the amplitude of the initial density fluctuation, and c_I (I = A, B, S) are the volume fractions of segment A, segment B, and solvent S, respectively. According to the strategy adopted by Balazs et al.,[32,33] the initial distribution of particle center $\rho_P(\mathbf{r})$ is uniform, which is used to calculate the local volume fractions of particles $\phi_P(\mathbf{r})$ and $\bar{\phi}_P(\mathbf{r})$ from eqs 3 and 8. The initial field $\omega_I(\mathbf{r})$ (I = A, B, S, P) are calculated by using eqs 9−12 (the initial incompressibility field $\xi(\mathbf{r})$ is set to be zero). For the solution of the diffusion equation (6), we employ the Baker−Hausdorff operator splitting formula proposed by Rasmussen et al.,[49,50] which has higher stability and accuracy than other methods for the same spatial discretization. The diffusion equation (6) is discretized according to

$$q(\mathbf{r},s+ds) = \exp\left[-\frac{ds}{2}\omega(\mathbf{r})\right] \exp[ds\,\nabla^2] \exp\left[-\frac{ds}{2}\omega(\mathbf{r})\right] q(\mathbf{r},s) + O(ds^3) \tag{19}$$

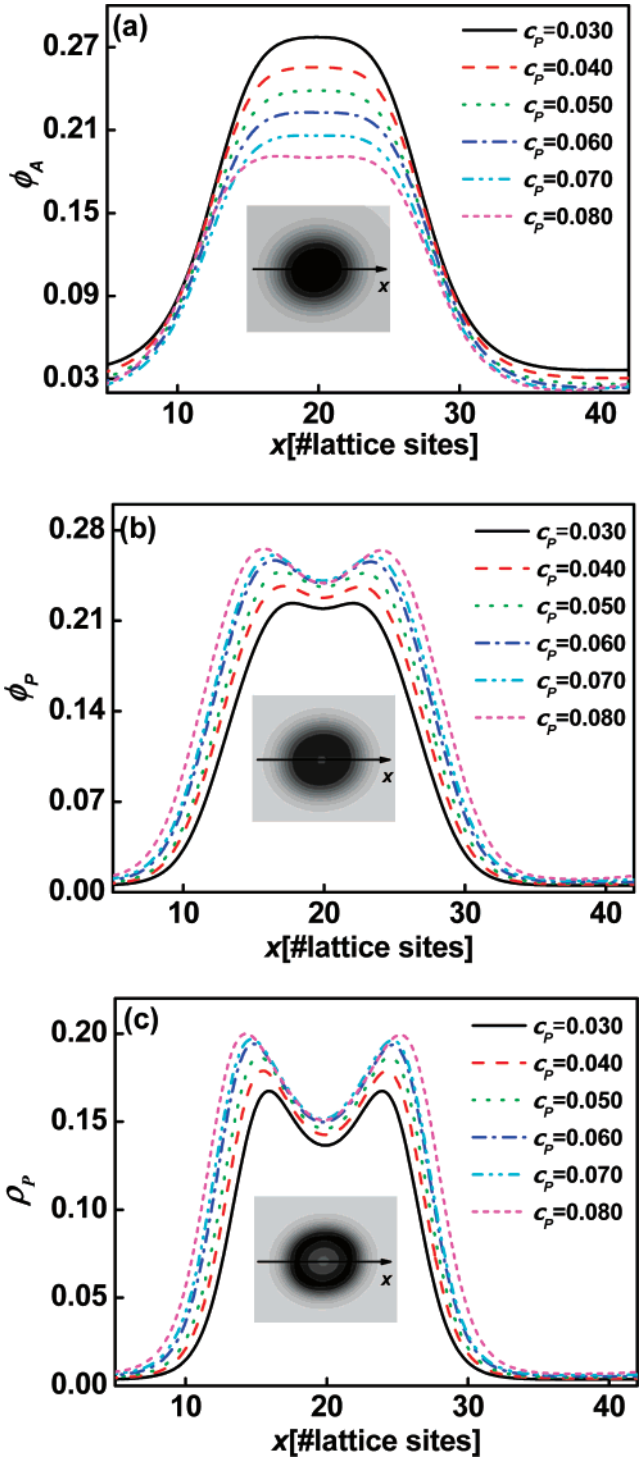

Figure 3. Distribution profiles of hydrophobic blocks ϕ_A (a), particles ϕ_P (b), and particle centers ρ_P (c) on a cross section of the circlelike micelle marked with an arrow in the inset with various particle volume fractions for $R_P/R_g = 0.70$. The inserts are two-dimensional distributions of hydrophobic blocks (a), particles (b), and particle centers (c) for $R_P/R_g = 0.70$ and $c_P = 0.080$.

The operator $\exp[-ds\omega(\mathbf{r})/2]$ is trivially implemented in real space, while the operator $\exp[-ds\nabla^2]$ is implemented exactly in Fourier transform domain of the spatial variable. A fast Fourier transformation (FFTW) package is applied in the evaluation of the diffusion operator to ensure precision and convergence.[51] Next, the right-hand sides of eqs 3 and 13−16 are evaluated to obtain new expression values for the local volume fractions $\phi_I(\mathbf{r})$ of species I. To ensure the incompressibility of the system, the effective pressure field $\xi(\mathbf{r})$ is obtained through solving eqs 9−11 and 17.[27] Finally, the potential fields $\omega_I(\mathbf{r})$ and pressure field $\xi(\mathbf{r})$ are updated using eqs 9−12 by means of a two-step Anderson mixing scheme.[52,53] The iteration steps are repeated until the free energy reaches a local minimum, where the self-assembled structure corresponds to a metastable state.[27,28] This iteration scheme represents a pseudodynamical process having the steepest descent paths on the free energy landscape to the nearest metastable solutions. This method can rapidly evolve a system to a free energy minimum satisfying some constraints, e.g., incompressibility.

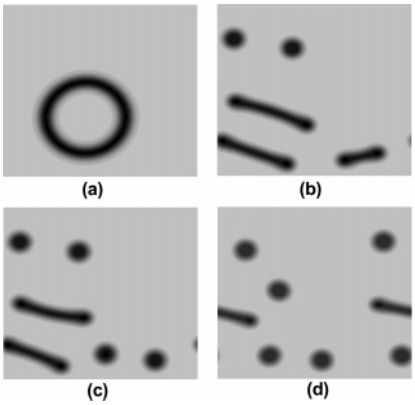

Figure 4. Two-dimensional density distributions of particles in the amphiphilic block copolymer/particle solutions with particle volume fraction $c_P = 0.025$ and particle radii $R_P/R_g = 0.65$ (a), $R_P/R_g = 0.72$ (b), $R_P/R_g = 0.75$ (c), and $R_P/R_g = 0.80$ (d). Light gray regions represent low local volume fraction of particles, while black regions indicate high local volume fraction of particles.

The SCFT calculations were performed in two dimensions on a 128 × 128 lattice with periodic boundary conditions. The contour's step size was set to be 0.01. The numerical simulation is carried out until the relative free energy changes at each iteration are smaller than 10^{-5} and the incompressibility condition is achieved. It is noted that the resulting aggregate morphologies depend on the amplitude of initial density fluctuation. As a result, the same initial density fluctuation amplitude was used in our simulations to ensure that the obtained morphologies are not affected by the initial fluctuation as it was done for the self-assembly of amphiphilic block copolymers in dilute solution in the literature.[27−30] In calculations, the simulations starting from a homogeneous copolymer solution were repeated for 10−20 times using different initial random states and different random numbers to ensure that the observed phenomena are not accidental.

Results and Discussion

In present simulations, the volume fraction of block copolymers c_D in solution is set as 0.08. The length of block copolymer chain is assumed to be $N = 25$. The composition of the hydrophobic part f_A is taken to be 0.86. The initial density fluctuation amplitude β is set to be 10^{-2}. We fix the invariant polymerization index $\bar{N}$ at 1.0 in all simulations. The SCFT/DFT studies reported below were carried out for the case that the particle size is smaller than the ideal gyration radius R_g of the diblock copolymer. The interaction parameter $\chi_{AB}N$ between the incompatible blocks A and B is set as 23.0. The A blocks and particles are hydrophobic. The interaction parameter between the A blocks and solvent and the interaction parameter between the particles and solvent adopt a value of 23.0 ($\chi_{AS}N = \chi_{PS}N = \chi_{AB}N = 23.0$). The B blocks are hydrophilic. The interaction parameter $\chi_{BS}N$ between the B blocks and solvent is set as zero. In terms of the particle selectivity, we

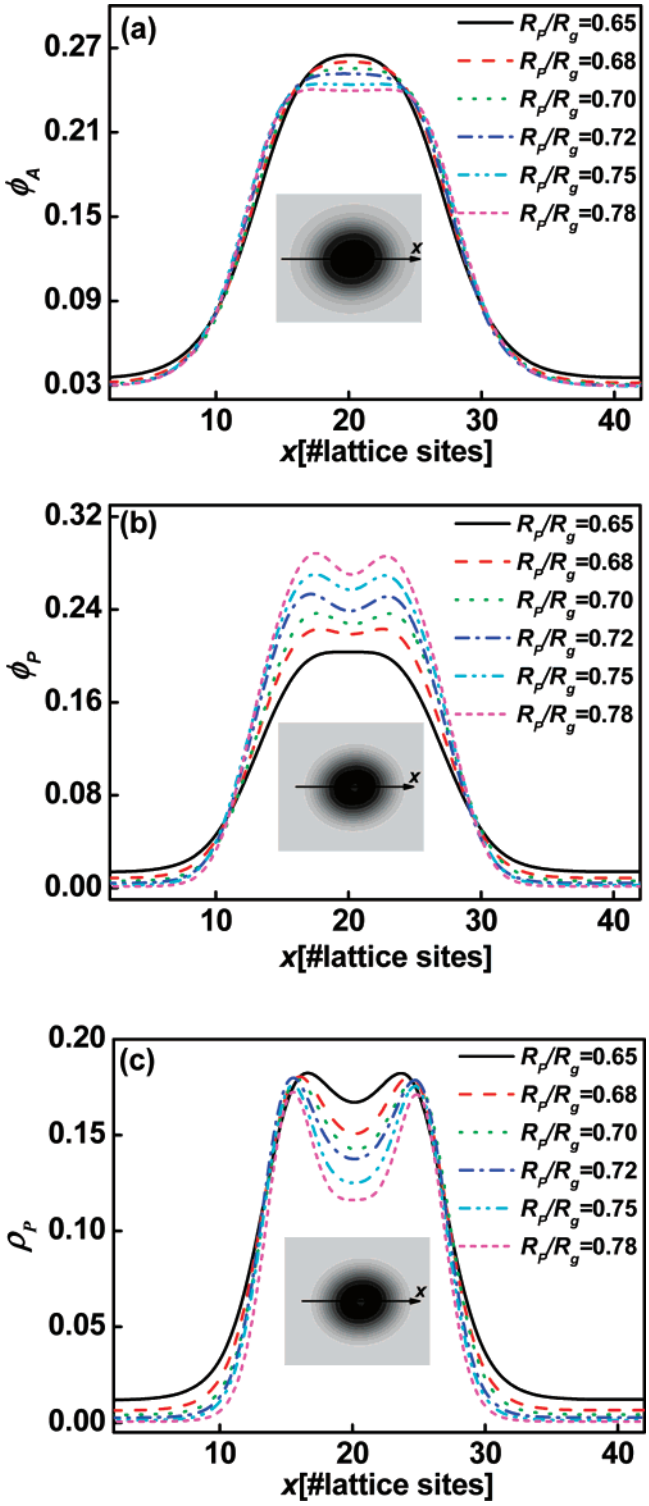

Figure 5. Distribution profiles of hydrophobic blocks ϕ_A (a), particles ϕ_P (b), and particle centers ρ_P (c) on a cross section of the circlelike micelle marked with an arrow in the inset with various particle radii for $c_P = 0.040$. The insets are two-dimensional distributions of hydrophobic blocks (a), particles (b), and particle centers (c) for $R_P/R_g = 0.78$ and $c_P = 0.040$.

studied two cases in our calculations. The particles are selective to the A blocks. To simplify the system and calculation, we take $\chi_{BP}N = 23.0$ and $\chi_{AP}N = 0.0$. The other scenario is that the particles are not selective to the A and B blocks. We assume $\chi_{AP}N = \chi_{BP}N = 0.0$. Under both conditions, the block copolymers do not associate themselves in dilute solution when the nanoparticles are not added into the system. In this work, we focus on the effects of volume fraction of particle c_P and

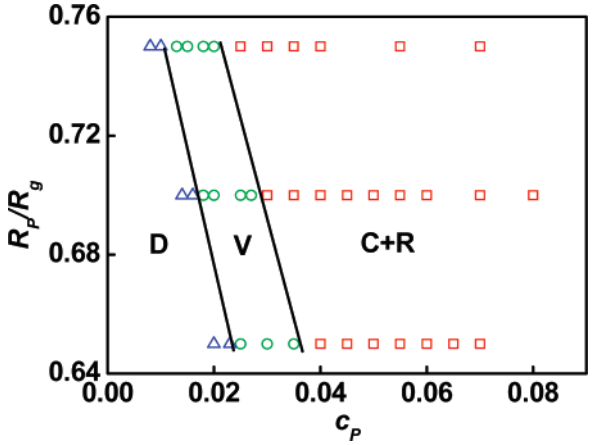

Figure 6. Aggregate morphology stability regions of amphiphilic block copolymer/nanoparticle solutions plotted as functions of particle radius R_P/R_g and particle volume fraction c_P. The notations D, V, and C + R represent the disorder state, vesicles, and mixture of circlelike and rod micelles, respectively. Each point in the phase diagram corresponds to a simulation result, and lines are drawn to identify the resulting phase boundaries.

radius of particle R_P on the aggregation behavior of diblock copolymer/nanoparticle mixture.

1. Selective Particles to A Blocks. In this subsection, we consider the effect of particle volume fraction and particle radius on the aggregate morphologies of diblock copolymer/nanoparticle mixture and the spatial distributions of particles in the aggregates. The interaction parameters $\chi_{AP}N$ and $\chi_{BP}N$ are set as 0.0 and 23.0, respectively. Under such a condition, the particles are preferentially wet to the A blocks.

Figure 1 shows the two-dimensional density profiles of particles with an increase in particle volume fraction for particle radius $R_P/R_g = 0.70$. Light gray regions represent low local volume fraction of particles, while black regions indicate high local volume fraction of particles. When the particle volume fraction is low, the particles are uniformly distributed in the system, and the aggregation of diblock copolymer/nanoparticle does not occur (not shown in Figure 1). As the particle volume fraction increases to 0.020, a vesicle forms and the particles are distributed in the wall of the vesicle, as shown in Figure 1a. The mixture of circlelike micelles and rod micelles appears with further increasing the particle volume fraction. The nanoparticles are encapsulated in the micelles (Figure 1b). When more particles are added into the solution, more micelles are formed in solution (Figure 1c,d).

As stated above, the self-association of amphiphilic block copolymer/nanoparticle mixture and the transition of aggregate morphologies can be triggered by increasing particle volume fraction. When the volume fraction of particle is lower, the nanoparticles and amphiphilic block copolymers are uniformly dispersed in the solution, and no aggregates are formed. As more particles are added into the system, the total free energy could significantly increase due to the increase in the total hydrophobic surface of nanoparticles. To depress such an effect and lower the total free energy, aggregates with hydrophobic blocks in the inner and hydrophilic blocks in the outer are formed and nanoparticles are migrated into the energetically favorable hydrophobic domains. It should be noted that these also result in the conformational entropy loss due to the confinement of copolymer chains and the translational entropy change due to the confinement of nanoparticles. Compared with the free energy contributed from entropy, the free energy from enthalpy dominates the aggregation process, resulting in the formation

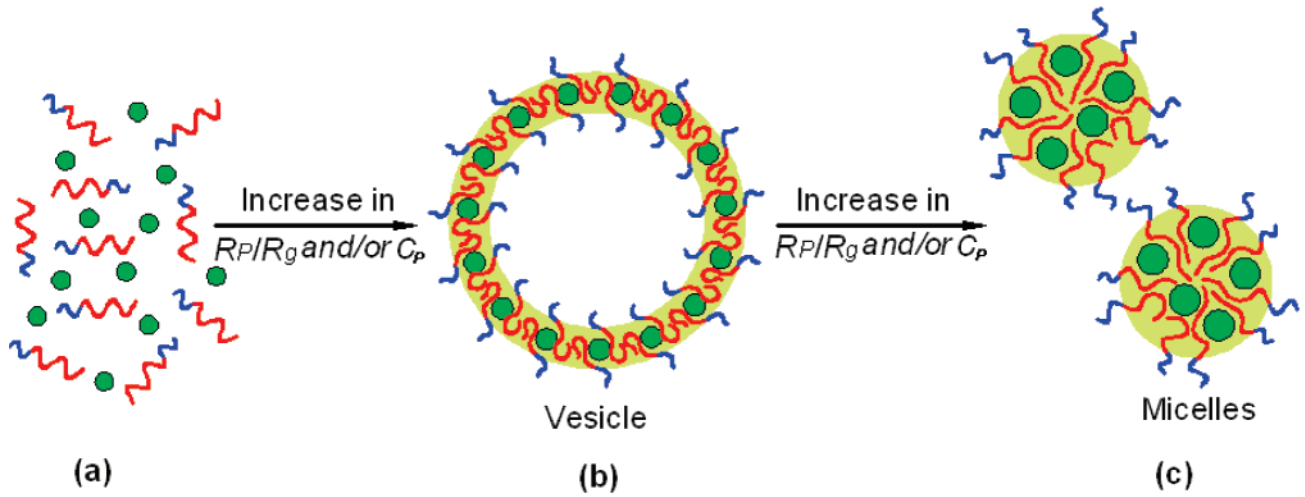

Figure 7. Schematic representations of the disorder state (a), vesicle (b), and micelles (c) for the amphiphilic diblock copolymer/nanoparticle system. The red lines, blue lines, and circles filled with green color denote the hydrophobic blocks, hydrophilic blocks, and nanoparticles, respectively. The solvent is not illustrated for clarification.

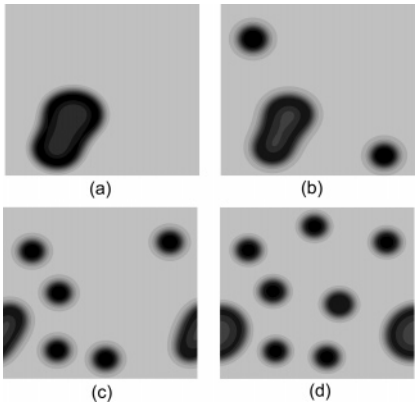

Figure 8. Two-dimensional density distributions of particles in the amphiphilic block copolymer/particle solutions with particle radius $R_P/R_g = 0.75$ and particle volume fractions $c_P = 0.020$ (a), $c_P = 0.022$ (b), $c_P = 0.025$ (c), and $c_P = 0.040$ (d).

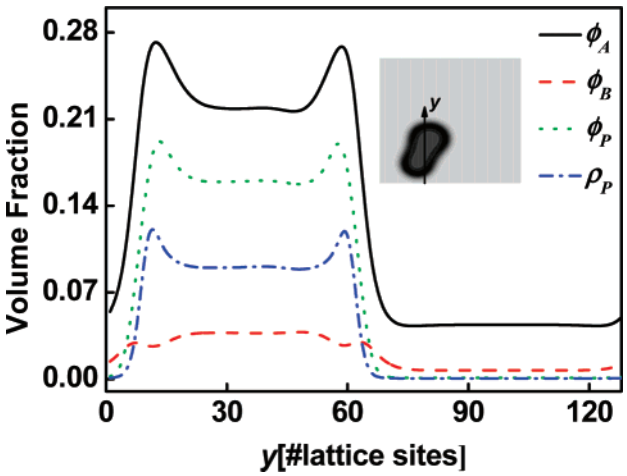

Figure 9. Distribution profiles of hydrophobic blocks ϕ_A, hydrophilic blocks ϕ_B, particles ϕ_P, and particle centers ρ_P on a cross section of the large compound micelle marked with an arrow in the inset for $R_P/R_g = 0.75$ and $c_P = 0.020$. The inset is two-dimensional density distribution of particles.

of the vesicles. When the aggregates are formed, the particles are sequestered in the hydrophobic parts of the aggregates and the steric packing effect of particles (which is a measure of the crowding of the hard particles) becomes predominant. As the particle volume fraction progressively increases, more clusters (from a vesicle to mixture of micelles) are produced in order to decrease the total free energy.

To obtain the detailed structure information on the aggregates, the density distributions of respective components in vesicles and circlelike micelles are plotted in Figure 2 and 3, respectively. The density profiles of hydrophobic blocks (ϕ_A), hydrophilic blocks (ϕ_B), particles (ϕ_P), and particle centers (ρ_P) in the vesicle are shown in Figure 2. The inset illustrates the two-dimensional density profile of particles. The profile of ϕ_A shows a bimodal feature, i.e., the hydrophobic blocks A form the wall of the vesicle. The inner and outer leaves of the vesicle are composed of hydrophilic blocks B. The peak position of particle distribution and peak position of particle center distribution are almost identical, and these profiles are symmetric with respective to the center of the wall. This indicates that the particles localize in the center of the vesicle wall.

As the particle volume fraction further increases, while the diblock copolymer volume fraction remains the same, the morphology transition from the vesicle to mixture of circle-like and rod micelles takes place. The density distributions of hydrophobic blocks (ϕ_A), particles (ϕ_P) and particle centers (ρ_P) are shown in Figure 3. The local volume fraction of hydrophobic blocks in the centers of circlelike micelles has a decrease with increasing the particle volume fraction (Figure 3a) due to the fact that the number of aggregates increases. Figure 3b shows the density distributions of particles. When the particle volume fraction is 0.030, the density profile of particles has almost a plateau in the center region of circlelike micelle, and the particles are well distributed in the core of the micelle. However, as the particle volume fraction increases, a cave in the center and two protrusions near the interface appear. The particles are accustomed to be far from the center region of aggregate in order to lower the steric packing effect of particles. This is also demonstrated by the distributions of particle centers (Figure 3c). There are a cave in the center region of the micelles and two protrusions near the interface. The protrusion positions of particle center distributions have a shift toward the interface between the core and the shell as the particle volume fraction increases.

Figure 4 is the two-dimensional density distributions of the particles obtained for the systems with various particle radii. The particle volume fraction is fixed at $c_P = 0.025$. When the particle radius is small, the aggregation of diblock copolymer/nanoparticle does not take place, and the particles are dispersed in the diblock copolymer solution uniformly. As particle radius increases to $0.65R_g$, a vesicle appears and the particles are distributed in the wall of the vesicle (Figure 4a). When the particles become larger further, the morphology transition from the vesicle to mixture of circlelike and rod micelles occurs (Figure 4b−d).

The distribution profiles of hydrophobic blocks (ϕ_A), particles (ϕ_P), and particle centers (ρ_P) for various particle radii in circlelike micelles are shown in Figure 5. As the particle radius increases, the local volume fraction of hydrophobic blocks in the core of micelles has a decrease (as shown in Figure 5a). It is ascribed to the fact that there are more micelles assembled by the copolymers, while the copolymer volume fraction is kept the same. The particle distributions are illustrated in Figure 5b. The local volume fraction of the particles in the micelles has an increase as the particle radius becomes larger. When the particle radius is $0.65R_g$, the particles almost uniformly mix with the hydrophobic blocks of diblock copolymers in the cores of the micelles. As the particle radius increases, a new feature of nanoparticle distributions in the aggregates is displayed. The larger nanoparticles are not homogeneously distributed. A cave in the center and two protrusions near the interface become gradually evident. Another noteworthy feature of these distributions is that the local volume fractions of particles outside the micelles decrease nearly to zero as the particle radius progressively increases. This suggests that an increase in the particle radius forces the particles into the micelles. As shown in Figure 5c, the particle center distribution has two protrusions near the interface and a cave in the center of micelles. With increasing the particle radius, the protrusion positions have a slightly shift toward interface between the core and the shell, and the cave turns much more evident.

To systemically capture the effect of particle radius and particle volume fraction on the aggregation behavior of the diblock copolymer/nanoparticle mixture, we plot the aggregate morphology stability regions for various values of particle radius R_P/R_g and particle volume fraction c_P, which are illustrated in Figure 6. Each point in the phase diagram corresponds to a simulation result, and lines are drawn to identify the resulting phase boundaries. The phase diagram is divided into three characteristic zones: disorder state (D), vesicles (V), and mixture of circlelike and rod micelles (C + R). Correspondingly, the disorder state, vesicles, and micelles are schematized in Figure 7. The red lines, blue lines, and circles filled with green color denote the hydrophobic blocks, hydrophilic blocks, and nanoparticles, respectively. The solvent is not illustrated for clarification. The phase diagram contains a disorder state at small values of particle radius and/or particle volume fraction. The hydrophobic nanoparticles and amphiphilic block copolymers are uniformly dispersed in solution (Figure 7a). With increasing the particle radius and/or particle volume fraction, the diblock copolymer chains and particles associate to form the vesicles, and the particles are positioned at the wall of the vesicles (Figure 7b). The transition from vesicles to mixture of circlelike and rod micelles is triggered by a further increase in particle radius and/or particle volume fraction. The nanoparticles are distributed in the cores of micelles (Figure 7c).

It is difficult at this time to make a comprehensive comparison between the theoretical predictions and experimental observations due to limited experimental studies on self-assembly behavior of mixture of amphiphilic block copolymers and nanoparticles in solution. However, we can still compare the calculation results with some existing experimental studies. Taton et al. reported the self-assembly of amphiphilic poly(styrene-*b*-acrylic acid)/nanoparticle mixture in dilute solution.[7,8] The amphiphilic block copolymer/nanoparticle mixture self-

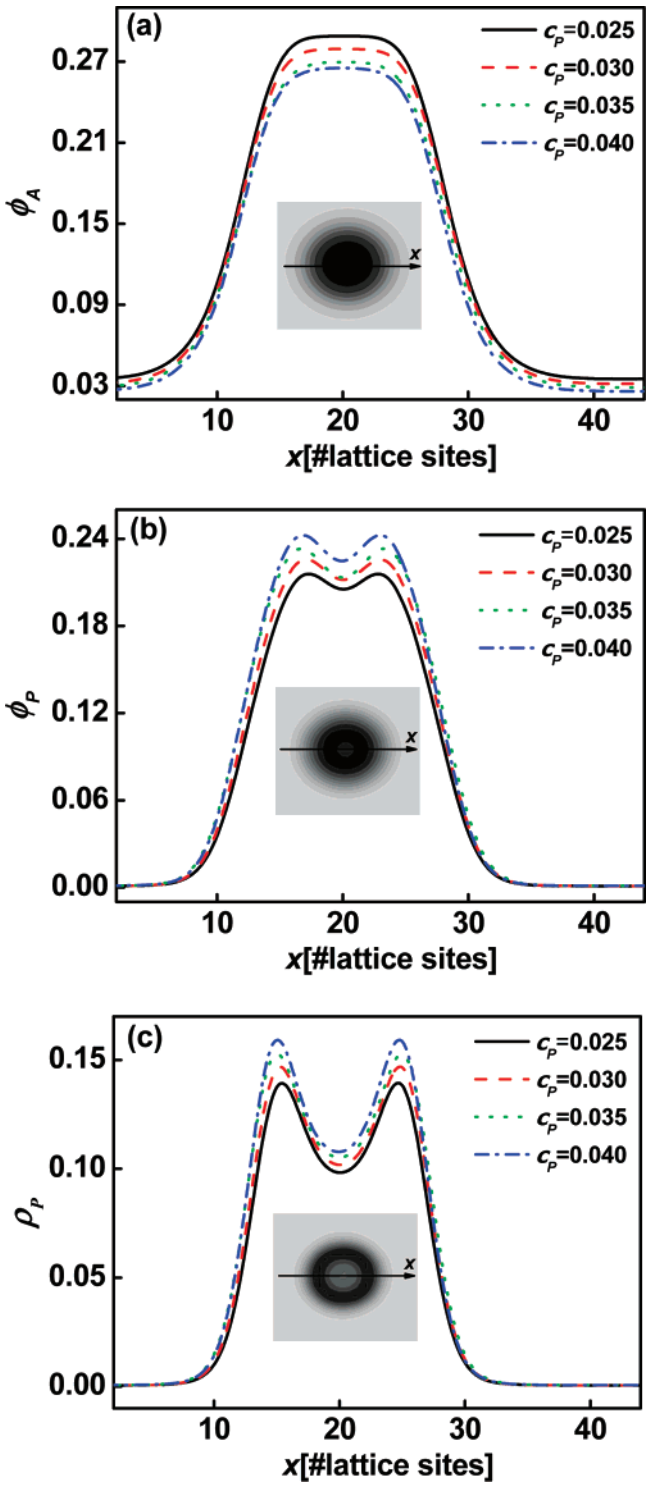

Figure 10. Distribution profiles of hydrophobic blocks ϕ_A (a), particles ϕ_P (b), and particle centers ρ_P (c) on a cross section of the circlelike micelle marked with an arrow in the inset with various particle volume fractions for $R_P/R_g = 0.75$. The inserts are two-dimensional distributions of hydrophobic blocks (a), particles (b), and particle centers (c) for $R_P/R_g = 0.75$ and $c_P = 0.040$.

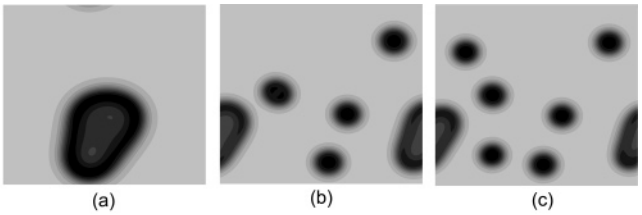

Figure 11. Two-dimensional density distributions of particles in the amphiphilic block copolymer/particle solutions with particle volume fraction $c_P = 0.03$ and particle radii $R_P/R_g = 0.65$ (a), $R_P/R_g = 0.68$ (b), and $R_P/R_g = 0.70$ (c).

associated to form the circlelike micelles, and the nanoparticles were encapsulated in the cores of micelles. With an increase in particle concentration at fixed polymer concentration, an increasing number of nanoparticles was encapsulated in each micelle and the average diameter of particle clusters became greater. Corresponding to our simulations, increasing the particle volume fraction gives rise to the greater local volume fraction of particles in the cores of micelles (as shown in Figure 3b). It is noteworthy that Thiyagarajan and co-workers recently examined the phase behavior of block copolymer/nanoparticle mixture in solution as functions of temperature and nanoparticle concentration.[54,55] They found that the transitions from lamellar → cylindrical → gyroid phases take place in block copolymer/nanoparticle complex solution with an increase in particle concentration, which differ from the lamellar → gyroid → cylindrical phase transition sequence in neat block copolymers with an increase in volume fraction of one segment of block copolymer. Although our simulations herein carried out in dilute solution, Figure 6 shows an analogous behavior that one can tune the particle volume fraction to yield various morphologies when the particle radius is fixed.

2. Nonselective Particles to A and B Blocks. In this subsection, we consider the case that the particles are nonselective to the A and B blocks. In this case, the interaction parameters $\chi_{AP}N$ and $\chi_{BP}N$ are set to be zero. The aggregate morphologies with an increase in the particle volume fraction are shown in Figure 8. When the amount of particles is less, the system is in a disordered state. As more particles are added into the solution, the particles induce the formation of large compound micelles (Figure 8a). With increasing the particle volume fraction, the transition from the large compound micelle to mixture of circlelike micelles and large compound micelle occurs (Figure 8b). Further increasing the particle volume fraction gives rise to an increase in the number of clusters (Figure 8c,d). Obviously, the nanoparticles with either selectivity or nonselectivity show a similar effect on the self-assembly behavior of amphiphilic block copolymer/nanoparticle mixture (Figures 1 and 8); i.e., the incorporation of nanoparticles leads to the formation of a large cluster, and more clusters are produced when the particle volume fraction further increases. However, as for the particles which are nonselective to the A and B blocks, the large compound micelles instead of the vesicles are formed.

The density profiles of hydrophobic blocks (ϕ_A), hydrophilic blocks (ϕ_B), particles (ϕ_P), and particle centers (ρ_P) for the large compound micelles are plotted in Figure 9. The outer shell of the aggregate is composed of the hydrophilic blocks B. In addition, the density profile of hydrophilic blocks B has a plateau in the center region of cluster, indicating that the structure also consists of some hydrophilic blocks in the center region of the cluster. The distributions of hydrophobic blocks and particles have a quasi-bimodal feature similar to the vesicles, with two

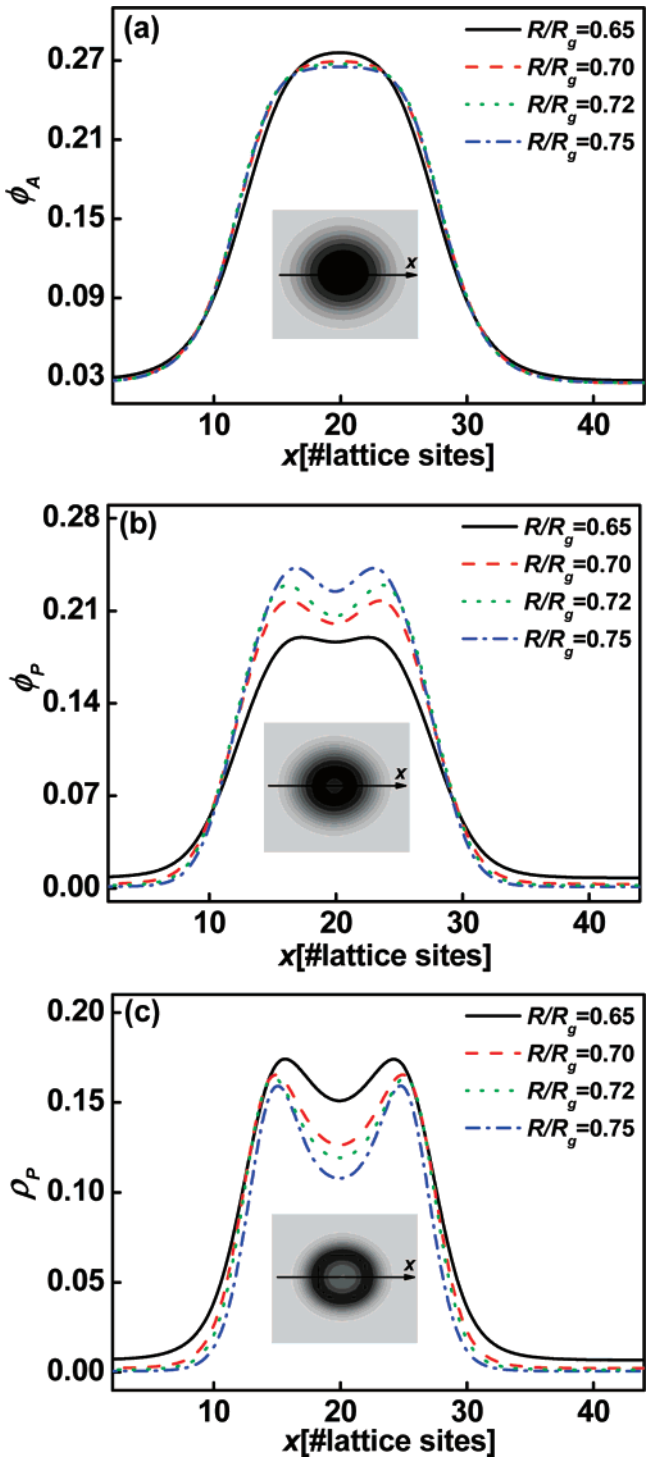

Figure 12. Distribution profiles of hydrophobic blocks ϕ_A (a), particles ϕ_P (b), and particle centers ρ_P (c) on a cross section of the circlelike micelle marked with an arrow in the inset with various particle radii for $c_P = 0.040$. The insets are two-dimensional distributions of hydrophobic blocks (a), particles (b), and particle centers (c) for $R_P/R_g = 0.75$ and $c_P = 0.040$.

small peaks at the interface and a plateau in the center region of the cluster. As the particle volume fraction increases above 0.025, the circlelike micelles appear in the system. Figure 10 shows the distributions of hydrophobic blocks (a), particles (b), and particle centers (c) in circlelike micelles with various particle volume fractions for particle radius $R_P = 0.75R_g$. As the particle volume fraction increases, more aggregates are formed to reduce the contribution of the steric packing energy of particles to the

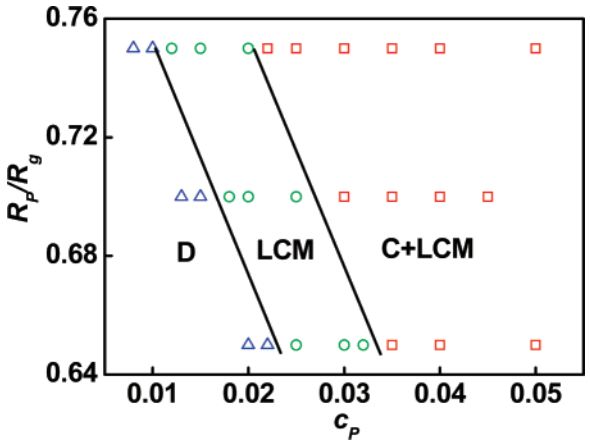

Figure 13. Aggregate morphology stability regions of amphiphilic diblock copolymer/nanoparticle solutions plotted as functions of particle radius R_P/R_g and particle volume fraction c_P. The notations D, LCM, and C+LCM represent the disorder state, large compound micelles, and mixture of circlelike and large compound micelles, respectively.

total free energy, which results in the less content of copolymers in the aggregate (Figure 10a). In addition, more particles are encapsulated in the aggregate. The cave and protrusions in both particle distribution and particle center distribution curves become marked, indicating that increasing particle volume fraction can induce the inhomogeneous distribution of particles (Figure 10b,c). The particles have a tendency to localize near the interface when more particles are added into the solution.

As illustrated in Figure 11, the dependence of the two-dimensional distribution of particles on the particle radius is plotted. As the particle radius increases, the particles can induce the self-association of block copolymers. A large compound micelle is formed at the small particle radius (Figure 11a). The transition from the large compound micelles to mixture of large compound micelles and circlelike micelles is triggered by an increase in the particle radius (Figure 11b,c). The distributions of hydrophobic blocks (a), particles (b), and particle centers (c) in circlelike micelles with various particle radii are illustrated in Figure 12. The content of hydrophobic blocks in the core of micelle has a decrease due to the formation of more aggregates in the system (Figure 12a). Meanwhile, the number of nanoparticles sequestered by the amphiphilic block copolymers has a marked increase. The smaller nanoparticles can be almost uniformly distributed in the core of the micelle. However, the distribution of the larger nanoparticles becomes inhomogeneous (Figure 12b,c). Accumulation of the simulation results indicates that variations in the size and volume fraction of particles can be exploited to tune the particle distribution in the aggregates.

We constructed the morphology stability regions for R_P/R_g and c_P, which are shown in Figure 13. Three characteristic zones are included in the phase diagram: disorder state (D), large compound micelles (LCM), and mixture of circlelike and large compound micelles (C+LCM). Correspondingly, the disordered state, large compound micelles, and mixture of large compound micelles and circlelike micelles are schematized in Figure 14. The mixture of nanoparticles, block copolymers, and solvent is in a disordered state at small values of particle volume fraction and/or particle radius (Figure 14a). The block copolymers form the large compound micelles, and the particles are accommodated in the clusters as the particle volume fraction and/or radius increase. As shown in Figure 14b, the large compound micelle consists of a hydrophilic outer shell, which stabilizes the hydrophobic part of aggregate. Because of the nonselectivity of particles to A and B blocks, the hydrophilic blocks can also migrate into the inner of the cluster. With further increasing the particle volume fraction and/or radius, more clusters including micelles and large compound micelles are produced (Figure 14c).

Some experimental evidence is available in the literature, supporting the simulation results of the large compound micelles assembled by the amphiphilic block copolymers and nanoparticles. Moffitt et al. prepared the large compound micelles in water by slowly adding water to blend solution of block copolymer stabilized CdS nanoparticles and amphiphilic block copolymers poly(styrene-*b*-acrylic acid) (PS-*b*-PAA).[56,57] Large compound micelles with nanoparticles encapsulated inside and hydrophilic PAA outer shells were observed. Corresponding to our simulations, the hydrophilic blocks form the outer shells to stabilize the large compound micelles, while the nanoparticles are positioned inside the aggregates. It should be noted that the large compound micelles can transform to vesicles as the interaction between nanoparticles and hydrophilic blocks becomes strong (Figures 7 and 14). Our studies not only reproduce the general features of experimental findings but also elucidate

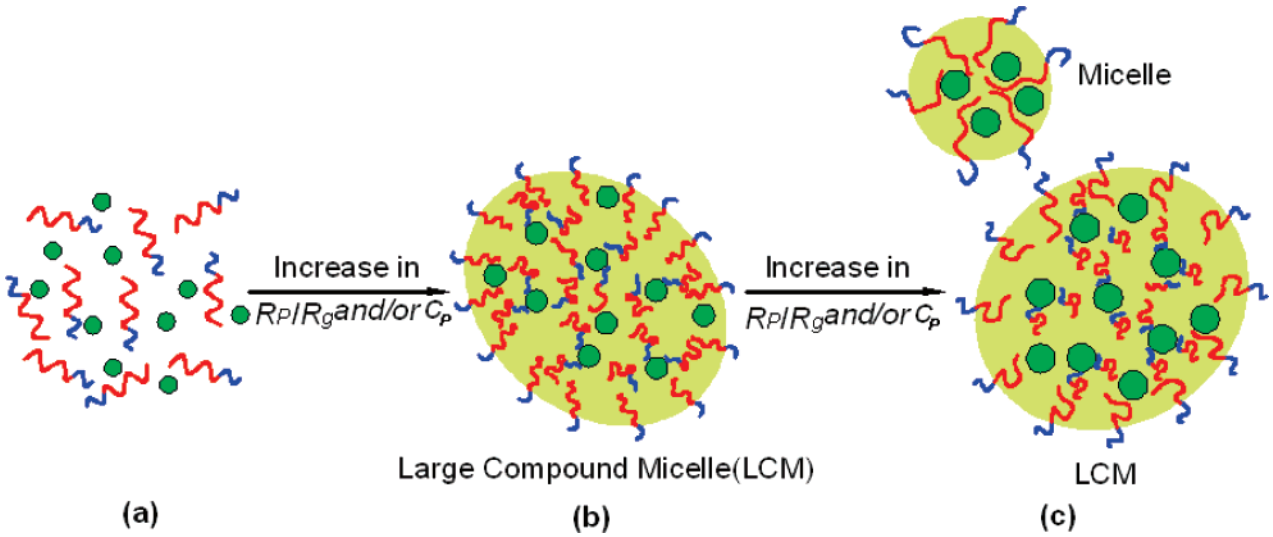

Figure 14. Schematic representations of the disorder state (a), large compound micelle (b), and mixture of large compound micelle and circlelike micelle (c) for amphiphilic diblock copolymer/nanoparticle solution.

the internal structural information on the large compound micelles.

Finally, it should be noted that the fluctuations, which are neglected in the formalism of mean-field theory, may cause alterations of the mean-field predictions. The fluctuation effects could become important for the solutions, especially dilute and semidilute.[58] The aggregate morphology stability regions of the amphiphilic block copolymer/nanoparticle solution in the present work may experience some degree of shifts when the fluctuations are considered. Therefore, our results should be treated more qualitative rather than quantitative. However, the mean-field theory is able to capture the essential features of the system, such as the aggregate morphologies and the nanoparticle distributions in the aggregates. Recent developments in field theoretic polymer simulation (FTPS) make FTPS possible to numerically sample the fluctuations in a complete model to accurately computer polymer structures and thermodynamic properties.[23,25,59,60] For example, the simulations have been used to examine the effect of fluctuations on the order−disorder transition in symmetrical diblock copolymer melts.[23] The order of magnitude of the fluctuation-induced shifts of the transition temperature is consistent with the analytical predictions obtained from a self-consistent Hartree analysis of fluctuation effects on the diblock copolymers.

Conclusions

We applied the SCFT/DFT method to study the self-assembly behavior of amphiphilic block copolymer/nanoparticle mixture in dilute solution. The particles are either selective to the hydrophobic A blocks or are not selective to the hydrophobic A and hydrophilic B blocks. In both cases, self-association of block copolymer/nanoparticle mixture takes place and the nanoparticles are encapsulated in the aggregates. For the A-selective particles, the aggregate morphologies of amphiphilic block copolymer/nanoparticle mixture can experience a transition from the vesicles to mixture of circlelike and rodlike micelles when the particle radius and/or particle volume fraction increase. For the nonselective nanoparticles, the block copolymer/nanoparticle mixture produces the large compound micelles instead of the vesicles and mixture of large compound micelles, and circlelike micelles are observed as the particle radius and/or particle volume fraction increase. We also present the local volume fraction distribution profiles of the respective components. The nanoparticles are almost uniformly distributed in the cores of micelles when the nanoparticles radius and/or number of encapsulated nanoparticles are small. However, the nanoparticles tend to localize near the interface between the core and shell as the particle radius and/or particle volume fraction increase.

Acknowledgment. This work was supported by National Natural Science Foundation of China (50673026, 20574018). Support from Doctoral Foundation of Education Ministry of China (Grant No. 20050251008), Program for New Century Excellent Talents in University in China (NCET-04-0410), and Project of Science and Technology Commission of Shanghai Municipality (05DJ14005, 06SU07002, and 0652nm021) is also appreciated.

References and Notes

(1) Hamley, I. W. *Block Copolymers in Solution: Fundamentals and Applications*; John Wiley & Sons: Chichester, UK, 2005.
(2) Lin, S.; Numasawa, N.; Nose, T.; Lin, J. *Macromolecules* **2007**, *40*, 1684−1692.
(3) Balazs, A. C.; Emrick, T.; Russell, T. P. *Science* **2006**, *314*, 1107−1110.
(4) Hamley, I. W. *Angew. Chem., Int. Ed.* **2003**, *42*, 1692−1712.
(5) Shenhar, R.; Norsten, T. B.; Rotello, V. M. *Adv. Mater.* **2005**, *17*, 657−669.
(6) Bockstaller, M. R.; Mickiewicz, R. A.; Thomas, E. L. *Adv. Mater.* **2005**, *17*, 1331−1349.
(7) Kang, Y.; Taton, T. A. *Angew. Chem., Int. Ed.* **2005**, *44*, 409−412.
(8) Kang, Y.; Taton, T. A. *Macromolecules* **2005**, *38*, 6115−6121.
(9) Kim, B.-S.; Qiu, J. M.; Wang, J.-P.; Taton, T. A. *Nano Lett.* **2005**, *5*, 1987−1991.
(10) Kim, B.-S.; Taton, T. A. *Langmuir* **2007**, *23*, 2198−2202.
(11) Zhang, Y.; Luo, S.; Liu, S. *Macromolecules* **2005**, *38*, 9813−9820.
(12) Euliss, L. E.; Grancharov, S. G.; O'Brien, S.; Deming, T. J.; Stucky, G. D.; Murray, C. B.; Held, G. A. *Nano Lett.* **2003**, *3*, 1489−1493.
(13) Loginova, T. P.; Kabachii, Y. A.; Sidorov, S. N.; Zhirov, D. N.; Valetsky, P. M.; Ezernitskaya, M. G.; Dybrovina, L. V.; Bragina, T. P.; Lependina, O. L.; Stein, B.; Bronstein, L. M. *Chem. Mater.* **2004**, *16*, 2369−2378.
(14) Zheng, P.; Jiang, X.; Zhang, X.; Zhang, W.; Shi, L. *Langmuir* **2006**, *22*, 9393−9396.
(15) Chen, S.; Guo, C.; Hu, G.-H.; Wang, J.; Ma, J.-H.; Liang, X.-F.; Zheng, L.; Liu, H.-Z. *Langmuir* **2006**, *22*, 9704−9711.
(16) Sakai, T.; Alexandridis, P. *Chem. Mater.* **2006**, *18*, 2577−2583.
(17) Bronstein, L. M.; Sidorov, S. N.; Zhirov, V.; Zhirov, D.; Kabachii, Y. A.; Kochev, S. Y.; Valetsky, P. M.; Stein, B.; Kiseleva, O. I.; Polyakov, S. N.; Shtykova, E. V.; Nikulina, E. V.; Svergun, D. I.; Khokhlov, A. R. *J. Phys. Chem. B* **2005**, *109*, 18786−18798.
(18) Luo, S.; Xu, J.; Zhang, Y.; Liu, S.; Wu, C. *J. Phys. Chem. B* **2005**, *109*, 22159−22166.
(19) Kim, B. J.; Chiu, J. J.; Yi, G.-R.; Pine, D. J.; Kramer, E. J. *Adv. Mater.* **2005**, *17*, 2618−2622.
(20) Yeh, S.-W.; Wei, K.-H.; Sun, Y.-S.; Jeng, U.-S.; Liang, K. S. *Macromolecules* **2005**, *38*, 6559−6565.
(21) Sun, Y.-S.; Jeng, U.-S.; Liang, K. S.; Yeh, S.-W.; Wei, K.-H. *Polymer* **2006**, *47*, 1101−1107.
(22) Drolet, F.; Fredrickson, G. H. *Phys. Rev. Lett.* **1999**, *83*, 4317−4320.
(23) Ganesan, V.; Fredrickson, G. H. *Europhys. Lett.* **2001**, *55*, 814−820.
(24) Drolet, F.; Fredrickson, G. H. *Macromolecules* **2001**, *34*, 5317−5324.
(25) Fredrickson, G. H.; Ganesan, V.; Drolet, F. *Macromolecules* **2002**, *35*, 16−39.
(26) Zhang, L.; Lin, J.; Lin, S. *J. Phys. Chem. B* **2007**, *111*, 351−357.
(27) He, X.; Liang, H.; Huang, L.; Pan, C. *J. Phys. Chem. B* **2004**, *108*, 1731−1735.
(28) Jiang, Y.; Chen, T.; Ye, F.; Liang, H.; Shi, A.-C. *Macromolecules* **2005**, *38*, 6710−6717.
(29) Wang, R.; Tang, P.; Qiu, F.; Yang, Y. *J. Phys. Chem. B* **2005**, *109*, 17120−17127.
(30) Ma, J.; Li, X.; Tang, P.; Yang, Y. *J. Phys. Chem. B* **2007**, *111*, 1552−1558.
(31) Zhang, L.; Lin, J.; Lin, S. *J. Phys. Chem. B* **2007**, in press.
(32) Thompson, R. B.; Ginzburg, V. V.; Matsen, M.; Balazs, A. C. *Science* **2001**, *292*, 2469−2472.
(33) Thompson, R. B.; Ginzburg, V. V.; Matsen, M.; Balazs, A. C. *Macromolecules* **2002**, *35*, 1060−1071.
(34) Lee, J. Y.; Thompson, R. B.; Jasnow, D.; Balazs, A. C. *Macromolecules* **2002**, *35*, 4855−4858.
(35) Lee, J. Y.; Thompson, R. B.; Jasnow, D.; Balazs, A. C. *Phys. Rev. Lett.* **2002**, *89*, 155503.
(36) Ren, C.; Ma, Y. *J. Am. Chem. Soc.* **2006**, *128*, 2733−2737.
(37) Thompson, R. B. *Phys. Rev. E* **2006**, *74*, 041501.
(38) Spontak, R. J.; Shankar, R.; Bowman, M. K.; Krishnan, A. S.; Hamersky, M. W.; Samseth, J.; Bockstaller, M. R.; Rasmussen, K. Ø. *Nano Lett.* **2006**, *6*, 2115−2120.
(39) Reister, E.; Fredricksion, G. H. *J. Chem. Phys.* **2005**, *123*, 214903.
(40) Sides, S. W.; Kim, B. J.; Kramer, E. J.; Fredricksion, G. H. *Phys. Rev. Lett.* **2006**, *96*, 250601.
(41) Huh, J.; Ginzburg, V. V.; Balazs, A. C. *Macromolecules* **2002**, *33*, 8085−8096.
(42) Wang, Q.; Nealey, P. F.; de Pablo, J. J. *J. Chem. Phys.* **2003**, *118*, 11278−11285.
(43) Pryamitsyn, V.; Ganesan, V. *Macromolecules* **2006**, *39*, 8499−8510.
(44) Schultz, A. J.; Hall, C. K.; Genzer, J. *Macromolecules* **2005**, *38*, 3007−3016.
(45) Kim, J. U.; O'Shaughnessy, B. *Phys. Rev. Lett.* **2002**, *89*, 238301.
(46) Kim, J. U.; O'Shaughnessy, B. *Macromolecules* **2006**, *39*, 413−425.
(47) Carnahan, N. F.; Starling, K. E. *J. Chem. Phys.* **1969**, *51*, 635−636.
(48) Tarazona, P. *Mol. Phys.* **1984**, *52*, 81−96.
(49) Tzeremes, G.; Rasmussen, K. Ø.; Lookman, T.; Saxena, A. *Phys. Rev. E* **2002**, *65*, 041806.

(50) Rasmussen, K. Ø.; Kalosakas, G. *J. Polym. Sci., Part B: Polym. Phys.* **2002**, *40*, 1777−1783.
(51) Frigo, M.; Johnson, S. G. *The Fast Fourier Transform in the West 2.1.3*; MIT: Cambridge, MA, 2000 (http://www.fftw.org).
(52) Eyert, V. *J. Comput. Phys.* **1996**, *124*, 271−285.
(53) Thompson, R. B.; Rasmussen, K. Ø.; Lookman, T. *J. Chem. Phys.* **2004**, *120*, 31−34.
(54) Lo, C.-T.; Lee, B.; Winans, R. E.; Thiyagarajan, P. *Macromolecules* **2006**, *39*, 6318−6320.
(55) Lo, C.-T.; Lee, B.; Winans, R. E.; Thiyagarajan, P. *Macromolecules* **2007**, *40*, 641−647.
(56) Moffitt, M.; Vali, H.; Eisenberg, A. *Chem. Mater.* **1998**, *10*, 1021−1028.
(57) Yusuf, H.; Kim, W.-G.; Lee, D. H.; Guo, Y.; Moffitt, M. G. *Langmuir* **2007**, *23*, 868−878.
(58) de Gennes, P. G. *Scaling Concepts in Polymer Physics*; Cornell University Press: Ithaca, NY, 1979.
(59) Duchs, D.; Ganesan, V.; Fredrickson, G. H.; Schmid, F. *Macromolecules* **2003**, *36*, 9237−9248.
(60) Alexander-Katz, A.; Fredrickson, G. H. *Macromolecules* **2007**, in press.

MA070986Y